

FSI SIMULATIONS OF AN AEROELASTIC SYSTEM WITH AERODYNAMIC NONLINEARITY

**MUHAMAD KHAIRIL HAFIZI BIN MOHD
ZORKIPLI**

UNIVERSITI SAINS MALAYSIA

2018

**FSI SIMULATION OF AN AEROELASTIC SYSTEM WITH
AERODYNAMIC NONLINEARITY**

by

MUHAMAD KHAIRIL HAFIZI BIN MOHD ZORKIPLI

**Thesis submitted in fulfilment of the
requirements for the Degree of
Master of Science**

July 2018

ACKNOWLEDGEMENT

Praise is exclusively to Allah. The Lord of the Universe and Peace is upon the Master of the Messengers, his family and companions.

I would like to express my sincere appreciation to my supervisor, Dr. Norizham Abdul Razak for his endless effort in the supervision and guidance which I received. He has not only been an inspiration in academia but also a prominent role model as well. It goes without saying that without the guidance, opportunities and challenges set forth by him, the opportunity to gain experience from this research would not have been made possible. In short, he is more than an academic supervisor.

I would also like to give special thanks to my family especially my parents, who is very supportive in helping me completing my research. The encouragements and motivations my parents gave me are most valued. The support I received from my research colleagues primarily Ahmad Farris and Hong Chen Lai also contributed greatly to my research work. Without you all, this work would have been a dull one.

Other Professors and technical staffs especially Madam Rohayu and Mr. Jamari in the School of Aerospace & Mechanical Engineering are extended family who has been a very positive influence in the development of this work. I would also like to thank my parents for instilling at a very young age the many important lessons and positive aspects of life, which plays a crucial role in who I am today.

Thank you all.

TABLE OF CONTENT

	Page
ACKNOWLEDGEMENT	i
TABLE OF CONTENTS	ii
LIST OF TABLES	vi
LIST OF FIGURES	vii
LIST OF ABBREVIATIONS	xi
ABSTRAK	xiii
ABSTRACT	xv
CHAPTER ONE: INTRODUCTION	
1.1 Aeroelasticity	1
1.1.1 Stall Flutter	3
1.2 Conceptual Theory	4
1.2.1 Dynamic	4
1.2.2 Reduced Frequency	4
1.2.3 Equation of motion	5
1.2.4 Limit Cycle Oscillation	6
1.2.5 Steady Aerodynamics Model	7
1.2.6 Quasi Steady Aerodynamic Model	8
1.2.7 Unsteady Aerodynamics Model	9
1.2.7.1 Wagner's Effect	10
1.2.7.2 Theodersen's Function	11
1.3 Flow Behaviour	11
1.3.1 Boundary Layer Separation	12

1.3.2	Separation induced transition	13
1.3.3	Vortex formation	15
1.4	Motivation	16
1.5	Objectives of the research	16
1.6	Thesis Organization	17

CHAPTER TWO: LITERATURE REVIEW

2.1	Experimental	18
2.2	Structural dynamics	19
2.2.1	General formulation	20
2.3	Semi empirical model	25
2.4	Analytical model	30
2.5	Potential Flow	33
2.6	Numerical Computational Fluid Dynamics	36
2.6.1	General formulation	38
2.6.1.1	Navier-Stokes and Continuity Equation	38
2.6.1.2	Basic Principle of Turbulence modelling	39
2.6.1.3	Reynolds Averaging	40
2.6.1.4	Boussinesq Approach	41
2.6.1.3	Pressure-velocity coupling	42
2.6.2	RANS Models	43
2.6.2.1	Standard k- ϵ Model.	43
2.6.2.2	Standard $k - \omega$ Model	44
2.6.2.3	Shear- Stress Transport (SST) $k - \omega$ Model	45
2.6.3	Mesh requirement	46
2.6.4	Specifying inlet turbulence level	47

2.7	Coupling method	50
2.8	Simulation Based on Concept of fluid-structure Interaction	54
2.9	Summary	56

CHAPTER THREE: COMPUTATIONAL METHODOLOGY AND VALIDATIONS

3.1	Structural dynamic solver	57
3.1.1	Aeroelastic modelling	57
3.2	Coupling	58
3.2.1	Newmark Beta Method	59
3.3	Mesh and boundary condition	60
3.4	Parameter setup	62
3.5	Validations	64
3.5.1	Structural solver validation	65
3.5.2	Grid study	67
3.5.3	Steady flow validation	72
3.5.4	Unsteady flow validation	74
3.5.5	Fluid Structure Interaction validation	75

CHAPTER FOUR: RESULTS AND DISCUSSIONS

4.1	Case EA at 18.6% of chord	82
4.1.1	Dynamic Behavior	82
4.1.2	Unsteady Aerodynamics Behavior	87
4.2	Case EA at the Leading Edge	93
4.2.1	Dynamics Behavior	93
4.2.2	Unsteady Aerodynamic Behavior	97

4.3	Case EA at 35% of chord	103
4.3.1	Dynamics Behavior	103
4.3.2	Unsteady Aerodynamics Behavior	107
4.4	Result summary	119

CHAPTER FIVE: CONCLUSIONS

5.1	Conclusion	123
5.2	Future works	124

REFERENCES	126
-------------------	-----

APPENDICES

LIST OF PUBLICATIONS

LIST OF TABLES

	Page
Table 1.1 Classification of flow unsteadiness	4
Table 3.1 Aeroelastic system parameters from experiment.	63
Table 3.2 Structural validation parameters	65
Table 3.3 Parameter of different meshes used	68
Table 3.4 Parameters for grid study cases.	68
Table 3.5 Steady flow validation parameters	73
Table 3.6 Unsteady flow validation parameters	75

LIST OF FIGURES

	Page
Figure 1.1 Collar's Aeroelastic Triangle.	2
Figure 1.2 Schematic of a spring-supported symmetric airfoil.	5
Figure 1.3 Limit cycle oscillations time response (Abdul Razak et al., 2012).	6
Figure 1.4 Lift coefficients for two different wing configuration.	8
Figure 1.5 Laminar separation bubble (O'Meara and Mueller, 1987).	14
Figure 3.1 Aeroelastic system physical model.	57
Figure 3.2 Calculation loop.	60
Figure 3.3 Computational domain and mesh details.	62
Figure 3.4 Free structural vibration responses plot for acceleration.	66
Figure 3.5 Free structural vibration responses plot for displacement.	67
Figure 3.6 Free structural vibration responses plot for velocity.	67
Figure 3.7 Lift coefficients obtained at different number of nodes.	69
Figure 3.8 Moment coefficients obtained at different number of nodes.	69
Figure 3.9 Comparison pressure coefficients for mesh A, B and C.	70
Figure 3.10 Comparison wall shear stress for mesh A, B and C.	71
Figure 3.11 Comparison pressure coefficients for mesh C, D and E.	71
Figure 3.12 Comparison wall shear stress for Mesh C, D and E.	72
Figure 3.13 Lift coefficients obtained from turbulence model, experiment and XFOIL.	73

Figure 3.14	Drag coefficients obtained from turbulence model, experiment and XFOIL.	74
Figure 3.15	Comparison lift coefficients between Theoderson's method and CFD method.	75
Figure 3.16	LCO pitch amplitude comparison between experimental (Poirel et al., 2008) and ANSYS Fluent numerical results at 18.6% EA.	76
Figure 3.17	LCO pitch frequency comparison between experimental (Poirel et al., 2008) and ANSYS Fluent numerical results at 18.6% EA.	76
Figure 3.18	LCO pitch frequency as a function of airspeed for simulation and experiments (Peristy, 2014) at 35% EA.	78
Figure 3.19	LCO pitch amplitudes as a function of airspeed for simulation and experiments (Peristy, 2014) at 35% EA.	79
Figure 4.1	Decay response time history at $V_{\infty}=6$ m/s SST k- ω Rk=6 simulation for elastic axis 18.6%.	83
Figure 4.2	LCO pitch response time history at $V_{\infty}=7$ m/s SST k- ω Rk=6 simulation for elastic axis 18.6%.	83
Figure 4.3	LCO pitch frequency as a function of airspeed for ANSYS Fluent numerical results at 18.6% EA.	84
Figure 4.4	LCO pitch amplitude as a function of airspeed for ANSYS Fluent numerical results at 18.6% EA.	85
Figure 4.5	LCO pitch response and aerodynamic moment coefficient time history at 18.6% EA for airspeed 7 m/s.	88
Figure 4.6	Cm-pitch angle plot at $V_{\infty}=7$ m/s for 18.6% EA. Simulation SST k- ω Rk=6.	89
Figure 4.7	Profiles of the τ_w and C_p at AOA = -0.4 degrees pitching down.	90
Figure 4.8	Profiles of the τ_w and C_p at AOA = 3.5 degrees pitching up.	91
Figure 4.9	Profiles of the τ_w and C_p at AOA = 4.0 degrees pitching up roughly maximum AOA.	91
Figure 4.10	Comparison turbulent viscosity ratio left $V_{\infty}=7$ m/s and right $V_{\infty}=11$ m/s.	93
Figure 4.11	Decay response time history at $V_{\infty}=7$ m/s SST k- ω Rk=6 simulation for leading edge EA.	94
Figure 4.12	LCO pitch responses time history for ANSYS Fluent simulation at $V_{\infty}=8.5$ m/s for leading edge EA.	94
Figure 4.13	LCO pitch frequency as a function of airspeed for ANSYS Fluent simulation at leading edge EA.	95

Figure 4.14	LCO pitch amplitude as a function of airspeed for ANSYS Fluent simulation at leading edge EA.	96
Figure 4.15	LCO pitch response and aerodynamic moment coefficient time history at leading edge EA at airspeed 8.5 m/s.	98
Figure 4.16	Cm-pitch angle plot at $V_{\infty}=8.5$ m/s for leading edge EA. Simulation SST k- ω Rk=6.	99
Figure 4.17	Cl-pitch angle plot at $V_{\infty}=8.5$ m/s for leading edge EA. Simulation SST k- ω Rk=6.	99
Figure 4.18	Viscosity contour, AOA= 2.0 degrees, pitching up.	101
Figure 4.19	Profiles of the τ_w and C_p at AOA = 2.0 degrees pitching up.	101
Figure 4.20	Viscosity contour, AOA= 4.0 degrees, pitching up roughly at maximum AOA.	102
Figure 4.21	Profiles of the τ_w and C_p at AOA = 3.6 degrees pitching up roughly maximum AOA.	102
Figure 4.22	LCO response time history at $V_{\infty}=8$ m/s SST k- ω Rk=6 simulation for elastic axis 35%.	104
Figure 4.23	LCO frequency as a function of airspeed for ANSYS Fluent simulation and INSFLOW simulation (Peristy, 2014) at 35% EA.	105
Figure 4.24	LCO amplitude as a function of airspeed for ANSYS Fluent simulation and INSFLOW simulation (Peristy, 2014) at 35% EA.	105
Figure 4.25	LCO pitch response and aerodynamic moment coefficient time history at elastic axis 35% for airspeed 8 m/s.	107
Figure 4.26	Cm-pitch angle plot at $V_{\infty}=8$ m/s for elastic axis 35%. ANSYS Fluent Simulation SST k- ω Rk=6.	109
Figure 4.27	Cl-pitch angle plot at $V_{\infty}=8$ m/s for elastic axis 35%. ANSYS Fluent Simulation SST k- ω Rk=6.	110
Figure 4.28	Viscosity contours, AOA = 29 degrees, pitching up at point (1).	112
Figure 4.29	Profiles of the τ_w and C_p at AOA = 29 degrees pitching up, at point (1).	112
Figure 4.30	Viscosity contours, AOA = 40 degrees, pitching up at point (2).	113
Figure 4.31	Profiles of the τ_w and C_p at AOA = 40 degrees pitching up, at point (2).	114
Figure 4.32	Viscosity contours, AOA = 42 degrees, roughly maximum AOA pitching up at point (3).	115

Figure 4.33	Profiles of the τ_w and C_p at AOA = 40 degrees roughly maximum pitching up, at point (3).	115
Figure 4.34	Viscosity contours, AOA = 31 degrees, pitching down at point (4).	116
Figure 4.35	Profiles of the τ_w and C_p at AOA = 31 degrees pitching down, at point (4).	117
Figure 4.36	Viscosity contours, AOA = 11 degrees, pitching down at point (5).	118
Figure 4.37	Profiles of the τ_w and C_p at AOA = 11 degrees pitching down, at point (5).	118
Figure 4.38	LCO pitch frequency as a function of airspeed for numerical solution at three different elastic axis.	119
Figure 4.39	LCO pitch amplitude as a function of airspeed for numerical solution at three different elastic axis.	120
Figure 4.40	Comparison LCO C_m -pitch plot for small amplitude oscillation at airspeed 9 m/s for 18.6% EA and leading edge EA.	121
Figure 4.41	LCO C_m -pitch plot for large amplitude oscillation at airspeed 8 m/s for 35% EA.	122

LIST OF ABBREVIATIONS

2D	Two dimensional
3D	Three dimensional
AC	Aerodynamic Center
AOA	Angle of Attack
CFD	Computational Fluid Dynamic
CSD	Computational Structural Dynamics
DES	Detached Eddy Simulation
DOF	Degree Of Freedom
EA	Elastic Axis
FEA	Finite Element Analysis
FEM	Finite Element Method
FSI	Fluid Structure Interaction
LAO	Large Amplitude Oscillation
LCO	Limit Cycle Oscillation
LES	Large Eddy Simulation
LEV	Leading Edge Vortex
LSB	Laminar Separation Bubble
PISO	Pressure Implicit with Splitting of Operator
RANS	Reynold Average Navier-Stokes
RMS	Root Mean Square
RSM	Reynold Stress Model
SAO	Small Amplitude Oscillation
SIMPLE	Semi Implicit Method for Pressure Linked Equations

SIMPLEC	Semi Implicit Method for Pressure Linked Equations Consistent
SST	Shear Stress Transport
UDF	User Defined Function
URANS	Unsteady Reynold Average Navier-Stokes
VLM	Vortex Lattice Method

FSI SIMULASI SISTEM AEROELASTIK DENGAN KETIDAKSAMAAN AERODINAMIK

ABSTRAK

Tesis ini membentangkan kajian sistem aeroelastik sebuah model NACA0012 rigid yang dipasang secara elastik dengan ketidaksamaan aerodinamik. Tingkah laku aeroelastik dari sayap dua dimensi berayun diperiksa dengan cara simulasi numerik. Simulasi NACA0012 dipelajari secara numerik melalui simulasi aeroelastic dua dimensi menggunakan ANSYS Fluent 16.1 untuk menilai tindak balas getaran aeroelastic pada paksi elastik yang berlainan dengan ketidaksamaan aerodinamik dan mendapati fenomena ketidaksamaan aerodinamik terhasil daripada pemisahan lapisan sempadan, pemisahan dan aliran lampiran semula di sekitar aerofoil. Simulasi menggunakan model RANS (SST) $k-\omega$ dengan pembetulan nombor Reynolds yang rendah untuk menangkap aliran fizikal di sekitar aerofoil. Interaksi struktur bendalir dinamik (FSI) dicapai melalui gabungan persamaan struktur gerakan dengan penyelesaian bendalir dalaman melalui utiliti fungsi (UDF) yang ditentukan oleh Fluent. Simulasi numerik dijalankan pada tiga kedudukan paksi elastik (EA) yang berbeza, 0% (titik depan), 18.6% dan 35% dari titik depan. Simulasi dijalankan pada julat kelajuan angin dari 4 m/s hingga 14 m/s. Hasilnya menunjukkan dua amplitud ayunan yang berlainan daripada tindak balas dinamik yang dihasilkan oleh sistem aeroelastik, di EA dari 0% (titik depan) dan 18.6% menghasilkan ayunan amplitud kecil (SAO) sementara pada paksi elastik 35% menghasilkan ayunan besar amplitud (LAO). Pengesahan simulasi numerik menunjukkan kecenderungan yang sama dengan hasil eksperimen dan didapati menghasilkan amplitud had ayunan kitaran (LCO) yang boleh dibandingkan. Dari aspek aliran aerodinamik, pemisahan lapisan sempadan laminar didapati memainkan peranan penting untuk ayunan yang mengekalkan ayunan dalam

ayunan amplitud kecil. Fenomena aliran pusaran, pemisahan aliran dan fenomena pengaliran lampiran semula dijumpai menyebabkan amplitud yang besar dan pusaran aliran yang terbalik di titik belakang aerofoil menyebabkan sayap bergerak dan mengekalkan kitaran ayunan.

FSI SIMULATION OF AN AEROELASTIC SYSTEM WITH AERODYNAMIC NONLINEARITY

ABSTRACT

This thesis presents a study of aeroelastic system of an elastically mounted rigid NACA0012 airfoil with aerodynamics nonlinearity. The aeroelastic behavior of a two dimensional wing oscillating is examined by means of numerical simulations. The simulation of NACA0012 is studied numerically through unsteady two-dimensional aeroelastic simulation using ANSYS Fluent 16.1 to evaluate the aeroelastic response of stall flutter at different elastic axis with aerodynamic nonlinearities and found that the aerodynamic nonlinearities are from boundary layer separation, the separation and reattachment of flow around the airfoil. The simulation employed RANS (SST) $k-\omega$ model with low Reynolds number correction to capture the physical flow around the airfoil. The dynamics fluid structure interaction (FSI) were achieved by coupling the structural equation of motion with an in-house fluid solver through defined function (UDF) utility in Fluent. Numerical simulations were ran through at three different elastic axis (EA) positions, 0% (leading edge), 18.6% and 35% from the leading edge. The simulations were ran through at free stream velocity range from 4m/s to 14m/s. The results showed two different oscillation amplitudes from the dynamic responses generated by the aeroelastic system of the airfoil, at EA of 0% (leading edge) and 18.6% produced small amplitude oscillation (SAO) while at 35% elastic axis produced large amplitude oscillations (LAO). The validation of numerical simulation showed trends which are similar to experiment results and are found to produce a reasonably comparable limit cycle oscillation (LCO) amplitudes. From the aerodynamic flow aspect, laminar boundary layer separation was found to play an important role for the oscillation sustaining the pitching oscillation in small amplitude oscillation. Leading

edge vortex, flow separation and reattachment flow phenomena was found which caused large amplitude oscillation and reversed flow vortices at the trailing edge of the airfoil caused the wing to pitch down and maintaining the oscillation cycle.

CHAPTER ONE

INTRODUCTION

1.1 Aeroelasticity

“Aeroelasticity” is a term used to represent the field of study concerned with the interaction between the deformation of an elastic structure in an airstream and the resulting aerodynamic force. Aeroelasticity can be categorized into two major categories, static and dynamic. Static aeroelasticity consists of the interaction between elastic and aerodynamic forces whereas the dynamic side involves the interaction of aerodynamic, elastic, and inertial forces. Aeroelastic phenomena can include several types of oscillations resulted from classical bending torsion flutter, stall flutter, buffeting and Limit Cycle Oscillations (LCO). Flutter is an example of an unstable self-excited vibration, and can arise under conditions of steady-state airflow. In the design of aircraft and aerospace components, design for aeroelastic performance is of fundamental importance, where if flutter vibration amplitude cannot be controlled, catastrophic structural failure can result. The classical airfoil flutter is a fundamental flow induced instability mechanism described as self-excited plunging and pitching oscillations of an airfoil subjected to airflow. One of the first fundamental studies considering the classical airfoil flutter was published by Theodorsen (Theodorsen, 1934) who obtained a closed-form solution of the flutter instability in the frequency domain with the experimental validation. Flutter of airplane wings or aircraft engine turbomachinery blades is a critical issue determining the reliability of the aircraft. The flutter phenomenon is the results of the fluid structural interaction and is usually involved with complicated phenomena such as the shock wave boundary layer interaction, flow separation, nonlinear limited cycle oscillation, etc. Accurate

prediction of the flutter is very challenging due to the complex physical phenomena and the required large amount of computation. The current study is an effort to develop the methodologies needed to achieve prediction of aircraft flutter. The best way to explain aeroelastic phenomena and interaction between forces mentioned is by observing at Collar's aeroelastic triangle (Collar, 1946) shown in Figure 1.1 In Figure 1.1, main disciplines of stability and control, structural dynamics and static aeroelasticity each caused from the interaction of two of the three forces. However, all three forces are required to interact for dynamic aeroelastic effects to happen.

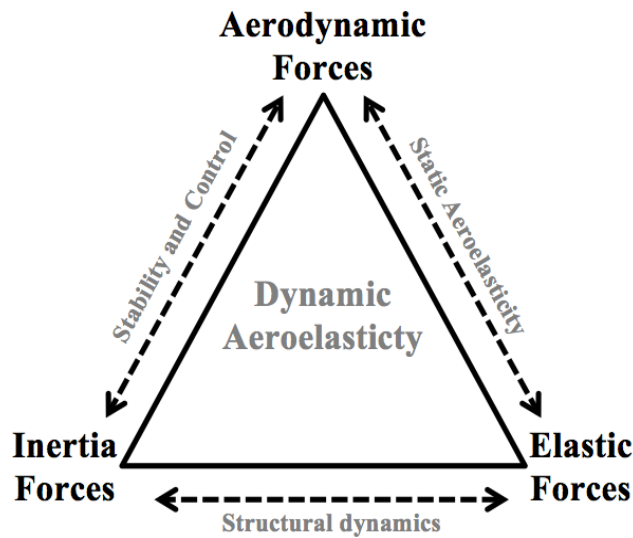


Figure 1.1: Collar's Aeroelastic Triangle

The presence of nonlinearity in aeroelastic system is known to affect the dynamic responses of the system which sometimes causes oscillation that cannot be predicted by linear theory (Razak, 2012). One of the types of oscillation is Limit Cycle Oscillation or LCO which requires at least one nonlinear element in a given system to occur. The sources of nonlinearity can be from structural or aerodynamic nonlinearities (Razak and Dimitriadis, 2013).

Computational fluid dynamics (CFD) and finite element method (FEM) provide the basic tools for predicting flutter, buffeting and limit cycle oscillation, hence computational aeroelasticity is expected to play a vital role in numerical modelling of combined solid-fluid interaction in the context of aerospace component and structure design (Schuster et al., 2003). In this project, Fluid structure interaction simulation analysis predicts the flow characteristics of the airfoil, including turbulence and flow separation.

1.1.1 Stall Flutter

Phenomenon of stall flutter arises when there is flow separation and reattachment to the surface of the wing in a cyclic manner. The separation can be categorized as partial separation or fully separation on the wing surface. Another aeroelastic phenomenon that can occur from the flow separation is galloping. The Occurrence of galloping can be observed when there is only flow separation over the bluff bodies. Dynamic stall is a process of alternation between stalled and attached flow, this phenomenon has been the subject of numerous experimental and theoretical investigations.(Ericson and Reding, 1971; McCroskey William, 1981; Spentzos et al., 2005)

The coupling of the vibration characteristics of a flexible structure with dynamic stall caused stall flutter to take place. The stall flutter phenomenon has been observed in helicopter rotor blades, wind turbine blades, low stiffness wing operating at high angles of attack and wind tunnel models.

1.2 Conceptual Theory

1.2.1 Dynamic

In this section the terminology that will be used to define airfoil, airfoil motions and unsteady aerodynamics in the rest of this thesis are presented. The terminology concerns geometric, aerodynamic and kinematic characteristics.

1.2.2 Reduced Frequency

In the field of aeroelasticity, reduced frequency describes the unsteadiness of the flow and is symbolized by the symbol k . Reduced frequency is a degree of flow unsteadiness due to body motion. Reduced frequency is given by

$$k = \frac{\omega b}{v} \quad (1.1)$$

Where, ω is the oscillation frequency, b is the airfoil's chord length and v is the free stream airspeed. The value of reduced frequency represents the unsteadiness of the flow which ranges from 0 to 1 as given in Table 1.1.

Table 1.1: Classification of flow unsteadiness

Range	Classification
$k = 0$	Steady
$0 < k < 0.05$	quasi-steady
$0.05 < k < 0.2$	Unsteady
$k > 0.2$	Highly unsteady

Reduced frequency values between 0 and 0.05 specifies quasi-steady flow where wake effects are unimportant. For 0.05 to 0.2 the flow is quasi-unsteady and added mass is negligible but wake effects are critical. The fully unsteady flow regime is characterized by reduced frequency values exceeding 0.2, the resulting flow is dominated by acceleration effects.

1.2.3 Equation of motion

Equation of motion for one degree of freedom can be obtained by applying summation of forces and moment acting on the airfoil body.

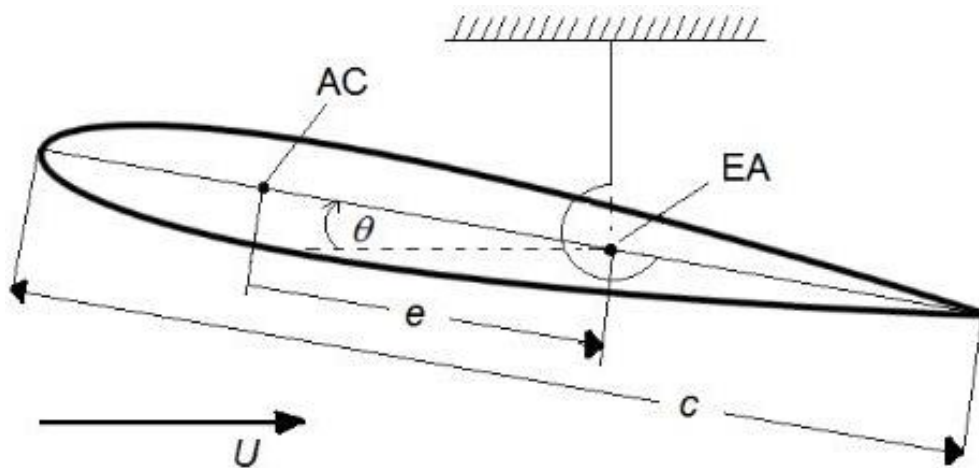


Figure 1.2: Schematic of a spring-supported symmetric airfoil.

From the Figure 1.2, AC is the aerodynamic center, EA is the elastic axis which the spring-supported symmetric airfoil is located, c is the chord length and e is the distance between aerodynamic center and elastic axis. In the case where the motion is restricted to pitching only, the equation of motion is given as:

$$I_{EA}\ddot{\theta} + D_{\theta}\dot{\theta} + K_{\theta}\theta = M_{EA} \quad (1.2)$$

Where, M_{EA} is the moment at the elastic axis, I_{EA} is the moment of inertia measured at the elastic axis, D_{θ} and K_{θ} are structural damping and structural stiffness respectively.

1.2.4 Limit Cycle Oscillation

Aeroelastic phenomenon are the dynamical phenomenon resulting from the mutual interaction of aerodynamic forces, elastic forces and elastic forces. Limit Cycle Oscillations (LCO) is one of the vibration phenomenon which requires at least one nonlinear element in a given system to occur (Razak and Dimitriadis, 2013). For an aeroelastic system, the nonlinearity can be from structural, aerodynamic or both. Flutter causes the system to vibrate and when nonlinearity elements is introduced, LCO phenomenon happens to sustain the vibration without any decay in the system. The nature of the transient oscillations is dependent on the initial conditions or perturbation given to the system.

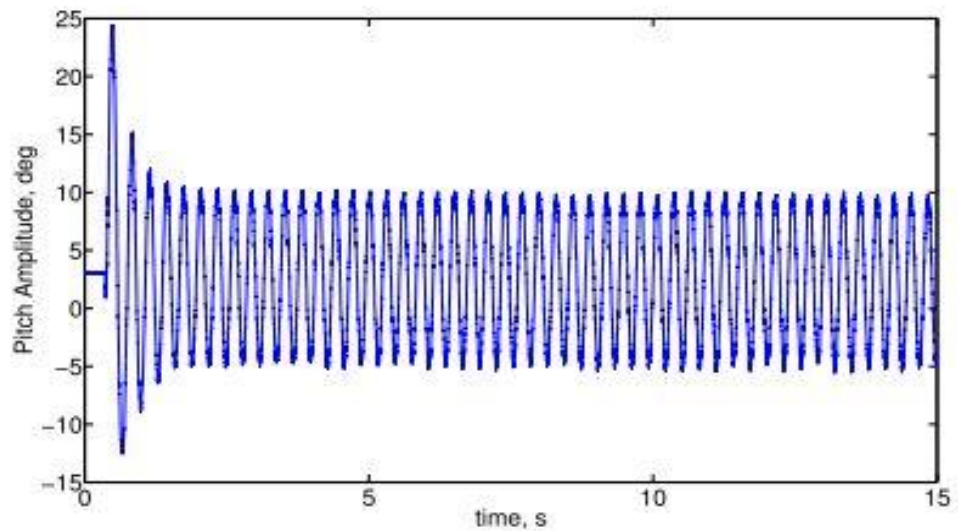


Figure 1.3: Limit cycle oscillations time response (Abdul Razak et al., 2012).